

Geoelectrical monitoring of simulated subsurface leakage to support high-hazard nuclear decommissioning at the Sellafield Site, UK



Oliver Kuras^{a,*}, Paul B. Wilkinson^a, Philip I. Meldrum^a, Lucy S. Oxby^a, Sebastian Uhlemann^{a,d}, Jonathan E. Chambers^a, Andrew Binley^b, James Graham^c, Nicholas T. Smith^{c,e}, Nick Atherton^f

^a British Geological Survey, Keyworth, Nottingham NG12 5GG, UK

^b Lancaster Environment Centre, Lancaster University, Lancaster LA1 4YQ, UK

^c National Nuclear Laboratory, Central Laboratory, Sellafield, Seascale, Cumbria CA20 1PG, UK

^d ETH-Swiss Federal Institute of Technology, Institute of Geophysics, Sonneggstr. 5, 8092 Zurich, Switzerland

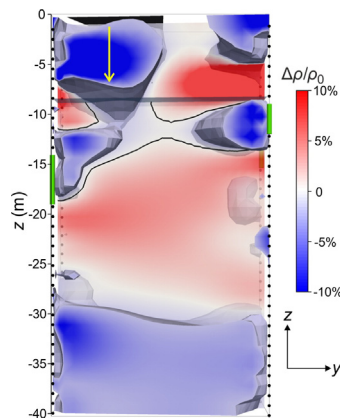
^e School of Earth, Atmospheric and Environmental Sciences, Williamson Building, University of Manchester, Oxford Road, Manchester M13 9PL, UK

^f Sellafield Ltd, Albion Square, Swingspump Lane, Whitehaven CA28 7NE, UK

HIGHLIGHTS

- 4D geoelectrical monitoring at Sellafield detected and tracked simulated silo leaks.
- ERT revealed likely pathways of silo liquor simulant flow in the subsurface.
- The method can reduce uncertainty in subsurface process models at nuclear sites.
- Has been applied in this form at a UK nuclear licensed site for the first time
- Study demonstrates value of 4D geophysics for nuclear decommissioning.

GRAPHICAL ABSTRACT



3D fractional resistivity change (resistivity change $\Delta\rho$ divided by baseline resistivity ρ_0) image showing results of Stage 1 silo liquor simulant injection. The black line delineates the preferential flow path; green cylinders show regions of historic contamination found in sediment cores from ERT boreholes.

ARTICLE INFO

Article history:

Received 14 October 2015

Received in revised form 27 April 2016

Accepted 28 April 2016

Available online xxx

Editor: D. Barcelo

Keywords:

Electrical resistivity tomography

Geophysics

Contaminant transport

ABSTRACT

A full-scale field experiment applying 4D (3D time-lapse) cross-borehole Electrical Resistivity Tomography (ERT) to the monitoring of simulated subsurface leakage was undertaken at a legacy nuclear waste silo at the Sellafield Site, UK. The experiment constituted the first application of geoelectrical monitoring in support of decommissioning work at a UK nuclear licensed site. Images of resistivity changes occurring since a baseline date prior to the simulated leaks revealed likely preferential pathways of silo liquor simulant flow in the vadose zone and upper groundwater system. Geophysical evidence was found to be compatible with historic contamination detected in permeable facies in sediment cores retrieved from the ERT boreholes. Results indicate that laterally discontinuous till units forming localized hydraulic barriers substantially affect flow patterns and contaminant transport in the shallow subsurface at Sellafield. We conclude that only geophysical imaging of the kind presented here has the potential to provide the detailed spatial and temporal information at the (sub-)meter scale needed to reduce the uncertainty in models of subsurface processes at nuclear sites.

* Corresponding author.

E-mail address: oku@bgs.ac.uk (O. Kuras).

1. Introduction

Whilst modern geophysical methodology is increasingly applied at nuclear legacy sites worldwide, the full potential of near-surface geophysics has yet to be fully recognized by the nuclear industry and its regulators. Recent studies have more frequently focused on characterizing historic contamination and hydrological processes (Johnson et al., 2012a; Johnson et al., 2012b; Slater et al., 2010), rather than directly supporting nuclear decommissioning activities (Calendine et al., 2011; Rucker et al., 2008). At the Sellafield Site in Cumbria, United Kingdom, major long-term decommissioning and remediation projects of national priority and international significance are currently underway that can demonstrably benefit from non-invasive subsurface monitoring approaches. The reduction of risk and hazard at four Sellafield plants known as the Legacy Ponds and Silos is a strategic priority for the UK's Nuclear Decommissioning Authority (NDA), but presents unique technical challenges. The safe emptying and decommissioning of the Magnox Swarf Storage Silos (MSSS) is a flagship project that Sellafield Ltd. are currently undertaking on behalf of the NDA. The complex and congested industrial setting of this facility demand the development and use of innovative decommissioning and monitoring technologies, both to prepare and to execute the retrieval of wastes from the silos (Nuclear Decommissioning Authority, 2011). The present study demonstrates the value of 4D subsurface geoelectrical monitoring in support of those efforts, and highlights its potential for underpinning risk management and environmental assurance for nuclear decommissioning programs.

1.1. Site history, leak scenarios and liquor properties

As nuclear generating capacity within the UK increased in the late 1950s, new Magnox reactors were built and enhanced waste management facilities were brought into service at Sellafield in the early 1960s. Fuel cladding and other solid wastes were stored in water-filled concrete silos (Baldwin, 2003), which over their 25-year operational life received Magnox swarf (debris from fuel decanning) and other wastes from nuclear sites across the UK. The original building was a simple reinforced concrete construction. Three later extensions increased capacity and introduced progressively improved containment standards. All material in the silos is submerged in water and much of the Magnox swarf has degraded into a sludge (BNFL, 1998).

During the 1970s, silo liquor is known to have leaked out of the original building, entering the ground below and creating a plume of contamination (BNFL, 2006). A rate of 3 m³/day has generally been accepted as the maximum measured rate of historic leakage. While none has been measured since, there is an increased risk that new leakage may occur during waste retrievals due to changes in structural loading caused by the installation and operation of waste retrieval equipment. The historic leak was originally discovered when contamination was identified in an adjacent excavation. Liquor balances have since been closely monitored and measurable leakage is thought to have occurred until 1980/81, when the estimated rate of liquor loss fell to the levels expected for evaporation only. A negative liquor balance of 5 m³/month (~0.17 m³/day) is currently regarded as the threshold for investigation.

Little information is available about the physical properties of the silo liquor and their variation over time. The electrical properties of the liquor are a function of the aqueous chemistry and temperature of the wastes and are expected to be controlled predominantly by the ionic concentrations of dissolved solids, however few samples have in the past been obtained from the silos, and those only at the liquor

surface. Electrical conductivities determined by lowering a sensor in the compartments fell in a range between 865 and 1940 $\mu\text{S}/\text{cm}$ (J Graham, pers. Comm.), but these may not be representative of the liquor properties at the base of the silos or at the point of entry into the geosphere.

1.2. Environmental monitoring at nuclear sites - a role for geophysics?

Environmental monitoring forms a key component of Sellafield Ltd.'s Ground Environment Management Scheme (GEMS) to assess the impact on groundwater contamination and risk to offsite receptors of contaminants from past and potential future leaks at the facility (Dewey et al., 2014). Prior research within the UK nuclear regulatory framework had highlighted the advantages of geophysical methodologies for leak mitigation (Cummings, 2012; Emptage et al., 2013). In particular, Electrical Resistivity Tomography (ERT) was identified as a preferential technology for in-ground detection and volumetric monitoring of potential subsurface leakage.

At an international level, there is also a growing body of research that has shown success with geoelectrical techniques for investigating leakage and contaminant transport at nuclear legacy sites, such as the Department of Energy's Hanford Nuclear Reservation in the United States (Daily et al., 2004; Johnson et al., 2012a; Johnson et al., 2012b; Ramirez et al., 1996; Rucker et al., 2008; Slater et al., 2010; Truex et al., 2013). In the UK however, ERT had never been used for leak detection at a nuclear licensed site before, and the much greater complexity of the site layout and geological setting at Sellafield compared to Hanford made a successful application of the method appear less likely. The near-surface geological setting at Hanford is dominated by a substantial vadose zone comprising coarse grained, Pleistocene-age cataclysmic flood deposits (the Hanford Formation, containing pebble-to-boulder-size gravels and interbedded sands) that are hydraulically permeable and electrically resistive (Slater et al., 2010). Typical contaminants at Hanford include liquids leaking from underground storage tank farms; unlike MSSS liquors, they are typically fully saturated saline solutions with very high electrical conductivity (Ramirez et al., 1996). The high property contrast between contaminants and geological background therefore lends itself well to the geophysical detection of plumes at Hanford.

Given the much more subtle contrasts expected at Sellafield, it was decided that a full-scale controlled field experiment should be undertaken at the facility, with the aims of assessing the suitability of ERT for leak detection, and monitoring and determining its 'Technology Readiness' (Mankins, 1995) for future permanent deployment at Sellafield and comparable sites. Predictive numerical simulations of possible subsurface leak scenarios had demonstrated the feasibility of the approach in principle (Kuras et al., 2011).

1.3. Geoelectrical monitoring with ERT

Direct Current (DC) resistivity (specifically ERT) is a key technique in the field of hydrogeophysics, which over the past 25 years has transformed 'our ability to see into the very fabric of the subsurface environment, and monitor the dynamics of fluids [...] that occur within it' (Binley et al., 2015). ERT monitoring methodology in particular has seen radical improvements (Loke et al., 2013a); without the most recent advances in data acquisition and inverse geophysical modelling the present study would have been inconceivable. ERT relies upon multiple and repeated measurements of bulk electrical resistance of the soil and subsurface deposits in the region of interest; these are carried out with a buried array of electrodes ('sensors') that must cover (as a minimum) the perimeter of the volume of ground to be monitored. Through

inverse modelling, ERT then transforms these measurements into volumetric images of ground resistivity. Resistivity is a fundamental geophysical property that is linked to hydrogeological properties and states through property relationships (Binley et al., 2015). Since it has a strong dependence on pore fluid saturation and dissolved contamination, changes in resistivity can be used to study the evolution of leakage plumes both in the vadose zone and in saturated groundwater bodies, provided the aqueous chemistry of the plume is significantly different to that of the native groundwater.

We present results for ERT monitoring of a series of controlled injection experiments, during which simulated silo liquor tracers were released into the vadose zone at locations, depth and release rates commensurate with those that might be expected of a real leak from the facility. The aim of this study is to demonstrate the effectiveness of 4D geoelectrical imaging as a flexible and powerful in-ground detection and volumetric monitoring tool that can provide subsurface information unavailable from conventional techniques, thus aiding the wider nuclear decommissioning effort at critical sites.

2. Materials and methods

2.1. Hydrogeological setting and implications for geophysical leak detection

A detailed understanding of the hydrogeology beneath the storage facility was essential for meaningful conceptualization and quantitative interpretation of tracer migration during the experiment. Much of the present level of geological knowledge about the site stems from the Sellafield Contaminated Land Study (SCLS) (Smith and Cooper, 2004) and follow-on investigation under the Sellafield Contaminated Land and Groundwater Management Project (Cruickshank, 2012). The conceptual ground model is shown in Fig. 1. Shallow bedrock beneath the site is of Triassic age and comprises the two uppermost lithostratigraphic units of the Sherwood Sandstone Group. Below the silos, bedrock is encountered at depths of ~40–45 m below ground level (bgl); at this location however, borehole information suggests the presence of a ‘trough’ in the bedrock surface topography, which is buried beneath superficial deposits of a comparatively greater thickness relative to adjacent areas of the Sellafield site. Superficial geology comprises Quaternary-aged deposits of variable thickness. A layer of made ground typically extends to depths of 1–3 m bgl, but greater thicknesses

are encountered in the direct vicinity of the silos where, during construction of the building, excavations exceeded a depth of 6 m bgl (the base of the silo foundations). Both the sandstone bedrock and the superfcials are of hydrogeological significance and classified as aquifers (El-Ghonemey, 2004). Superficial deposits are the principal medium through which contaminant transport occurs in the ground (Smith and Cooper, 2004). Partially saturated conditions prevail in the vadose zone, which is expected to be the primary region of entry into the geosphere for any leakage from the building. The water table below the silos is located at approximately 9–10 m bgl and shows only moderate seasonal variation (typically ± 1 m).

The surviving Quaternary sediments can be attributed to the last major glaciation that affected West Cumbria (the Devensian glaciation: 26–10 ka BP (Merritt and Auton, 2000)), and comprise a complex sequence of glacial and postglacial deposits including tills, alluvial sands and lacustrine sediments. The system has been divided into sixteen hydrostratigraphic units, whose relationship with lithological units (mappable lithofacies as well as lithostratigraphic units used in the 3D geological model of the site) is summarized in Table S1 (Supplementary information). It should be noted that the ‘3D model lithostratigraphy’ referred to here was created purely for modelling purposes using definition of lithofacies units, and in separation to the regional Quaternary lithostratigraphy of Merritt and Auton (2000). Of key hydrological significance is the depth and lateral extent of clay- and/or silt-dominated lithologies that are suspected to restrict vertical permeability at least locally, and, where present, act as barriers to the downward migration of groundwater and associated contaminant transport.

A low-permeability layer (‘Glacial till extensive aquitard unit’ below ~20 m bgl) is responsible for a high degree of hydraulic separation between upper and lower groundwater systems in the superficial deposits (El-Ghonemey, 2004) (Fig. 1). Groundwater in the lower Quaternary system is generally in connection with groundwater in the underlying sandstone, and together they are referred to as ‘lower (regional) aquifer’ in Fig. 1. Piezometric surfaces constructed for the upper and lower (regional) groundwaters using data from monitoring boreholes surrounding the experimental site had suggested contrasting patterns in average (site-scale) groundwater flow, with flow in the upper aquifer approximately to the east and flow in the regional aquifer approximately to the south-west.

However, the Quaternary deposits at Sellafield are highly variable and not laterally continuous, thus, it is generally difficult to predict hydraulic properties and resulting flow regimes in the shallow subsurface at the scale of an individual building. Simplified predictive models of the groundwater flow and tracer injection that incorporated the available geological knowledge at the time, suggested that a plume was likely to be detectable in the majority of scenarios considered (Kuras et al., 2011). However, that study used a generic translation of hydrological state (tracer concentrations) to geophysical properties (bulk resistivity), whose practical validity is likely to be limited.

The desire to robustly assess the performance of a geoelectrical leak detection system therefore made an in-situ experiment imperative. A central objective of the latter was to enhance our conceptualization of the hydrogeology at the silo facility and to improve our understanding of contaminant transport and likely plume behavior in the shallow subsurface at relevant (meter to sub-meter) scales. Given the difficulty, and hence scarcity, of intrusive investigations in this environment, the ERT experiment offered a unique opportunity to incorporate new borehole lithological information into the geological model of the site.

2.2. Experimental design

At the core of our experiment were three controlled injections into the vadose zone of environmentally benign, electrically conductive simulant fluids, continually monitored by automated cross-borehole ERT measurements at daily intervals. The simulants comprised saline tracer solution as a proxy for the silo liquor, and were developed to

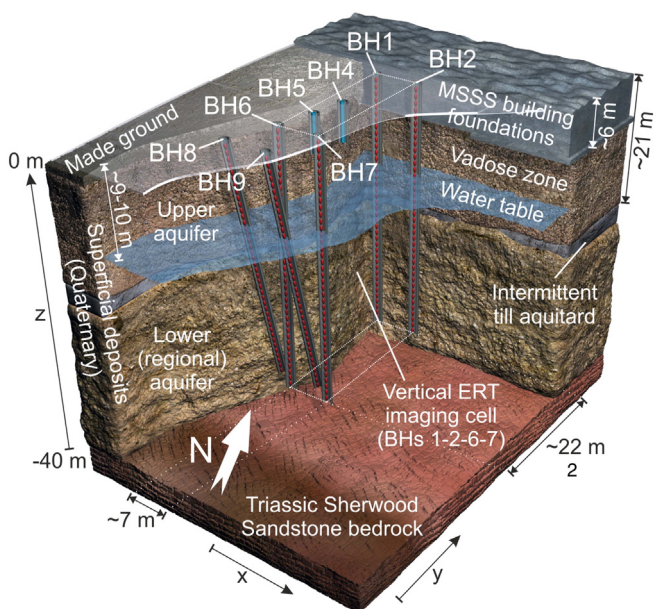


Fig. 1. Conceptual ground model and geometry of ERT borehole sensor arrays deployed at the silo facility.

replicate the range of measured conductivities. The three injections simulated leaks from the base of the silo foundations of moderate electrolytic conductivity contrast (3:1 compared to groundwater conductivity) at a typical leak rate of $\sim 0.7 \text{ m}^3/\text{day}$ (Stage 1); low contrast (2:1) at $\sim 0.7 \text{ m}^3/\text{day}$ (Stage 2); and higher contrast (5:1) at a high (hypothetical) leak rate of $\sim 10.8 \text{ m}^3/\text{day}$ (Stage 3). The Stage 1 injection was designed to last for an intermediate period (38 days) and occur from a location nearer the edge of the building (BH5); the Stage 2 injection lasted a longer time (97 days) and occurred from the building center (BH4); and the Stage 3 injection simulated a more significant leak over a short period (3 days, BH5). A detailed overview of the experimental parameters is given in Table S2 (Supplementary information).

Sellafield process water was used as the basis for the solutions. This process water was dosed with NaCl and NaBr to specific conductivities of $850 \mu\text{S}/\text{cm}$, $550 \mu\text{S}/\text{cm}$ and $1500 \mu\text{S}/\text{cm}$ at 25°C , respectively. A target molar ratio of Cl:Br of 10:1 (mass ratio of 4.4:1) was used in order to make the solution sufficiently distinct from the known Sellafield groundwater chemistry.

The experimental procedure covered six key practical steps, including (1) the drilling of boreholes and the installation of the ERT equipment, (2) baseline ERT monitoring to assess the ambient noise conditions at the site, (3) Stage 1 simulant injection and continual ERT monitoring, (4) ERT monitoring to study the decay of the Stage 1 plume and to re-baseline the system, (5) Stage 2 simulant injection, with any remnant Stage 1 plume remaining in the ground, and (6) Stage 3 simulant injection ('high flow'). Finally, extended ERT baseline monitoring was undertaken to capture plume decay and assess seasonal variation of external parameters (noise, sensor health, hydrology).

2.3. Borehole ERT sensor array geometry

Leak detection and monitoring at the silo facility required a focus on regions at or below the base of the building foundations, and ideally a non-destructive capability to detect and characterize potential leakage plumes beneath the building itself. A cross-borehole configuration of ERT sensors fulfills these criteria, with sensors located along boreholes situated on both sides of the building. However, sensitivity and resolution in crosshole ERT imaging are closely linked to and constrained by the separation between boreholes. The aspect ratio for a crosshole panel (separation between boreholes divided by length of electrode string in each borehole) should not exceed 0.75 in order to provide satisfactory image resolution (LaBrecque et al., 1996b). The most favorable imaging conditions are expected for ratios below 0.5 (Wilkinson et al., 2010). The limiting distance for borehole deployment at the silos is the width of the building that is $\sim 18 \text{ m}$. Boreholes could not be installed within $\sim 2 \text{ m}$ of the silo walls, so a minimum 'cross-building' borehole separation of 22 m had to be considered for our experiment. A lateral borehole spacing along the building walls of 7 m was chosen based on realistic numbers of boreholes required for a future monitoring installation covering the original building and first extension.

Below the older sections of the silo facility that are expected to have a greater potential for leakage due to their outdated design and building standards, the silo foundations extend to approximately 6 m bgl, which is well above the water table. Monitoring variations in fluid saturation, determining likely pathways and tracking the direction and timing of fluid flow between this depth and the water table is of particular interest for leak characterization at the facility. Due to the lack of detailed hydrogeological information, it was unclear how quickly any potential contaminant plume would migrate and how deep it would eventually sink. For the purposes of the ERT experiment it was therefore decided to include the entire sequence of superficial deposits in the initial monitoring strategy. Boreholes were therefore extended down to bedrock at $\sim 40 \text{ m}$ bgl, which also helped satisfy the geometric condition for imaging discussed above (aspect ratio achieved ~ 0.55).

Downhole ERT sensor arrays in six boreholes adjacent to the MSSS structure, but offset to the south, were arranged in an approximately

rectangular fashion, simulating deployment on opposite sides of the building (Fig. 1 and Fig. S1, Supplementary information). Four of the boreholes (BH1, 2, 6, 7) were vertical and represented the fundamental ERT imaging cell. Note that we use the term 'imaging cell' to refer to the parameter space bounded by four boreholes (one in each corner). Two further boreholes (BH8, 9) were installed at $\sim 12^\circ$ inclination and oriented perpendicularly towards the silo wall, in order to test deployment in areas of the original building where surface access was more restricted. These, together with the two vertical boreholes adjacent to the Silo (BH1, 2) formed a separate 'inclined imaging cell', for which the geometry was known from simulations to be less favorable. Each sensor array comprised 40 low-carbon grade austenitic stainless steel (UNS S31603) tubular electrodes with an exposed surface area of $\sim 44 \text{ cm}^2$, spaced at 1 m separations, resulting in a total of 240 buried sensors available for ERT imaging. Two shallow boreholes (6 m length) for simulant injection were placed between the four deep vertical boreholes. BH4 was located near the center of the area, approximately halfway between the borehole panels BH1–BH2 and BH6–BH7. BH5 was located closer towards the BH6–BH7 panel, at a distance of approximately 4.7 m from BH4. Simulant was injected at a depth of 6 m bgl in either borehole, simulating possible leak locations at the base of the silo foundations (see Table S2, Supplementary information).

2.4. Borehole and ERT system installation

The six ERT boreholes and two shallow injection boreholes were installed by rota-sonic drilling between August and October 2012 (Fig. S2, Supplementary information). Temporary steel casing was initially deployed in each borehole. ERT sensor cables mounted onto flexible PVC carrier tubing were carefully lowered into the open boreholes. The casings were then gradually withdrawn, whilst simultaneously backfilling the borehole annulus with extruded bentonite sealing pellets prepared from naturally occurring high purity montmorillonite (sodium activated bentonite). Given the ability of bentonite to swell and self-seal when hydrated by natural waters (here: the groundwater column in the open borehole), this procedure resulted in sensor emplacement that was mechanically stable and provided good galvanic contact between electrodes and the surrounding sediments. Moreover, the hydraulic sealing properties of the bentonite packer were essential to satisfy regulatory requirements. Performance tests showed that only three electrodes out of the 240 installed needed to be excluded from ERT measurements due to poor electrical contact.

Some concerns were raised over the impact of bentonite in the borehole column related to potential current shorting effects due to its low bulk resistivity ($\sim 2.5 \Omega\text{m}$ when saturated with deionized water in the laboratory), and to potential bias in the ERT measurements as a result of induced polarization (IP; ground charging phenomenon) effects associated with the complex conductivity of clays (Okay et al., 2014). However, predictive ERT modelling showed that shorting effects were acceptable and the use of a switched-DC source signal, combined with suppression of early time windows for potential measurements, helped reduce the risk of IP-related bias.

After the boreholes were completed, sensor arrays were connected to BGS-designed geoelectrical monitoring instrumentation known as ALERT technology (Kuras et al., 2009; Ogilvy et al., 2009; Wilkinson et al., 2010) that was installed in an environmental enclosure at the site. System batteries were recharged from grid power; this arrangement allowed automated scheduled collection of large electrical resistance datasets over long monitoring periods without operator intervention at site. A telemetric link via broadband internet to the BGS offices in Nottingham, UK, enabled fully remote operation and management of the ERT system, including upload of command schedules and regular (daily) download of datasets for analysis and interpretation.

2.5. ERT baseline measurements and variability assessment

Initial testing of the ERT system focused on an assessment of data quality that could be expected at the site. As was anticipated in the complex industrial environment at Sellafield, spurious electrical potentials were found to affect the measured data to varying degrees at different times. These potentials were suspected to be a combination of spontaneous potential (SP; electrical fields unrelated to the ERT current injection) and IP effects. In order to reduce their impact on monitoring the processes of interest, the measurement scheme was reorganized, and specific electrodes were excluded from further measurements (2 for vertical/inclined imaging cells and 2 further for inclined only).

After system commissioning, a 2-week period of quiescent baseline measurements was undertaken (20th Jan. – 2nd Feb. 2013), during which no further changes to the setup were made. Throughout the experiment, data acquisition on vertical and inclined imaging cells was scheduled separately on alternating days. A comprehensive measurement sequence was programmed for each cell, resulting in a total number of four-point resistance measurements per dataset of ~53,100. Crosshole bipole-bipole configurations were used (instead of configurations with current electrodes in a common hole and potential electrodes in a common hole), as they are known to be less sensitive to previously mentioned borehole effects (Chambers et al., 2007), for example the presence of an electrically conductive bentonite packer. Measurements contained reciprocal configurations (LaBrecque et al., 1996a), where the current and potential dipoles are swapped to assess the reciprocity of the resistance measurement. This allowed the calculation of ~13,400 averaged reciprocal measurements per dataset. The typical measurement duration per imaging cell was approximately 22.5 h; this time combined with data retrieval and transmission to the BGS servers meant that a routine 24-h measurement cycle could be achieved at the silo facility.

Error estimates from reciprocal measurements (timescale ~several hours) were compared with apparent resistivity variations in the data over the baseline measurement period (timescale ~several weeks), in order to understand short-term and long-term variability at the site under baseline ('no leak') conditions (Fig. 2). Short term variability (blue histograms) was found to be very low, with reciprocal error distributions peaking below 0.1%. Longer term variability of resistivities (orange histograms) was found to be significantly greater, but still acceptable compared with the levels of change caused by simulated leaks that were forecast by desk study numerical models (Kuras et al., 2011). Weather variations (air temperature and rainfall) for the ERT

experiment are shown in Fig. S3 (Supplementary information). Over the 2-week quiescent baseline period, they included temperature variations typical for the time of year (average air temperature $3.9^\circ \pm 2.7^\circ$) and total rainfall of ~40 mm. These are not considered major changes, but sufficiently large to be at least partially responsible for the longer term variability observed. Likely effects on the vadose zone electrical response as a result of precipitation-driven soil moisture variations are discussed in Section 3.2.

2.6. Simulant injection

Once baseline measurements were complete, controlled tracer injections were carried out from a purpose-built pump and tank skid installed near the boreholes. Details of injection timings, indicative duration and simulant properties are described in Table S2 (Supplementary information). Stage 1 and 2 injections were performed 'blind', i.e. the start date and time of the injections were controlled by Sellafield Ltd. and remained unknown to the ERT monitoring team. Continuously repeated ERT cross-borehole measurements using the vertical and inclined imaging cells were made before, during and after the injections allowing us to assess the information content of the ERT data with respect to both the occurrence of the simulated leak as well as the fate of the resulting plume.

2.7. ERT data processing

The relative complexity of the Quaternary geology at Sellafield, combined with the presence of clay-rich, electrically conductive sediments, result in limited electrical property contrasts between silo liquor, groundwater and site geology. This was seen as a major constraint for the success of geoelectrical methods at the silo facility. We also recognized that previous applications of ERT to nuclear waste leak detection reported in the literature were subject to significantly more favorable geological and geometrical conditions, for example at Hanford (Daily et al., 2004). Moreover, leak detection based on ERT is challenging in any circumstance as competing (but unrelated) environmental processes are known to affect bulk resistivity, including natural or man-made soil temperature variations, infiltration of surface water into the vadose zone, and electrical noise from plant operation and natural sources.

Nevertheless, initial efforts at MSSS included an attempt to perform leak detection based upon raw resistance data statistics alone, as such an approach had been successfully demonstrated at Hanford (Barnett

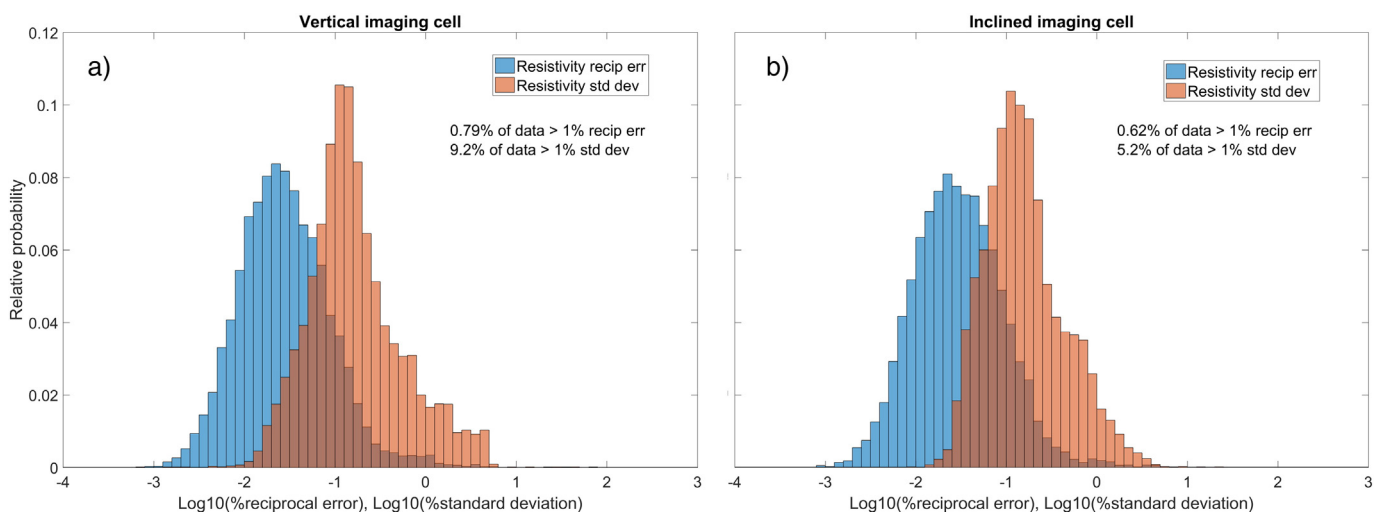


Fig. 2. Distributions of the reciprocal error (blue) and apparent resistivity standard deviation (orange) during baseline acquisition, providing measures for short-term variability and for longer-term variability in the study data, respectively. Distributions are shown for (a) vertical and (b) inclined imaging cells (based on 7 ERT datasets each). The reciprocal error is defined as the standard error of the mean of forward (fwd) and reciprocal (rec) measurement, $RE = 100|(\rho_{fwd} - \rho_{rec})/(\rho_{fwd} + \rho_{rec})|$.

et al., 2003; Daily et al., 2004). However, the results of an equivalent analysis at Sellafield were deemed unreliable, and consequently we proceeded by carrying out full 4D ERT inversion (3D time-lapse) to generate volumetric, time-dependent resistivity images of the subsurface in the trial area for further analysis. A 4D spatially and temporally smoothness-constrained inversion algorithm (Res3DInvX64 code by Geotomo Software, Malaysia) was used, implementing the method proposed in (Kim et al., 2009; Loke et al., 2013b). Our inversions used a model discretization based on a non-uniform rectangular grid to account for the borehole surface locations not being located on a regular grid pattern.

3. Results and discussion

3.1. Array sensitivity and baseline model

Given the constraints encountered with placing ERT boreholes at and around the silo building, the sensitivity for the inverse problem (McGillivray and Oldenburg, 1990) is known to vary significantly across the subsurface volume bounded by the ERT sensor array, with the central part of that volume having significantly lower sensitivity than the regions closer to the boreholes themselves. The cumulative sensitivity patterns for the entire field measurement set on the vertical and inclined imaging cells are shown in Fig. 3.

Absolute images of resistivity obtained during the baseline period (Fig. 4) reflected the heterogeneity of the geological setting at the site, but recovered electrical property distributions broadly compatible with the conceptual ground model (Fig. 1), subject to sensitivity constraints (Fig. 3). The images were also found to correlate well with stratigraphic logs obtained from the inspection of sediment cores from ERT boreholes. Whilst absolute resistivity images can be expected to be sensitive to saturation state, detailed saturation profiles have not been obtained at Sellafield, and uncertainty remains over actual saturation levels within the vadose zone below MSSS. A sharp decrease in resistivity is observed at ~7–9 m bgl in both BH1–2 and BH6–7 cross-hole panels (right-hand side of Fig. 4), likely associated with an increase in saturation levels near the water table. However, strong dependence of resistivity on sediment texture (particularly clay content) can also be expected. In the absence of a petrophysical model for Sellafield sediments, the arising ambiguity is best resolved by focusing on the analysis of resistivity change images.

3.2. Simulant injections and analysis by progressive stages

3.2.1. Quiescent baseline

3D fractional resistivity change during the quiescent baseline period and as a result of the Stage 1, 2 and 3 injections is shown in Fig. 5. 4D inverse modelling was performed at regular intervals, and the results were plotted as % changes relative to the inverted model at the start of the most recent injection stage (change in inverted resistivity at time t divided by inverted resistivity at baseline time). The quiescent baseline results (Fig. 5a) show that resistivity changes over that period are confined to the very shallow subsurface (upper vadose zone). Virtually no changes are observed in the saturated zone, and few isolated changes in the lower vadose zone. It is therefore reasonable to assume that the changes are largely associated with weather variations during the quiescent baseline period, possibly caused by shallow infiltration of rainfall (see Section 2.5) in unpaved areas of the experimental site.

3.2.2. Stage 1 injection

Simulant with a moderate electrical conductivity contrast was injected via BH5, but at a low leak rate. After ~4 weeks of continued injection for Stage 1, a consistent picture emerged; regions of increased conductivity developing in the time-lapse ERT images had strengthened in contrast and formed a coherent volume in the vadose zone and upper saturated zone, bounded by the 0% change contour (Fig. 5b). Its location was consistent with the known injection point (base of BH5, yellow arrow) and the assumption that the simulant plume will experience gravitational sinking due to its greater density, whilst broadly responding to the ambient lateral hydraulic gradients of the shallow groundwater system. Whilst the ERT images will allow interpretation of flow patterns on the scale of the imaging cell, deduction of more regional (site-scale) flow directions from one cell alone is not possible – only additional ERT boreholes (e.g. multiple imaging cells) could provide a capability to determine the fate of the plume on a larger (site) scale.

The strongest features of conductive change in the upper saturated zone were imaged in the immediate vicinity of ERT boreholes 1, 2, and 7 within narrow depth ranges that were consistent with windows of historic contamination (green cylinders), which had been detected in gravel-dominated (and hence likely more permeable) facies within sediment core recovered from the boreholes. No changes had been observed in this region during the quiescent baseline. This led us to infer the presence of a preferential hydraulic flow path, which appears to have been occupied by contaminants leaking from the silo facility in the past, and which has subsequently been re-occupied by the Stage 1

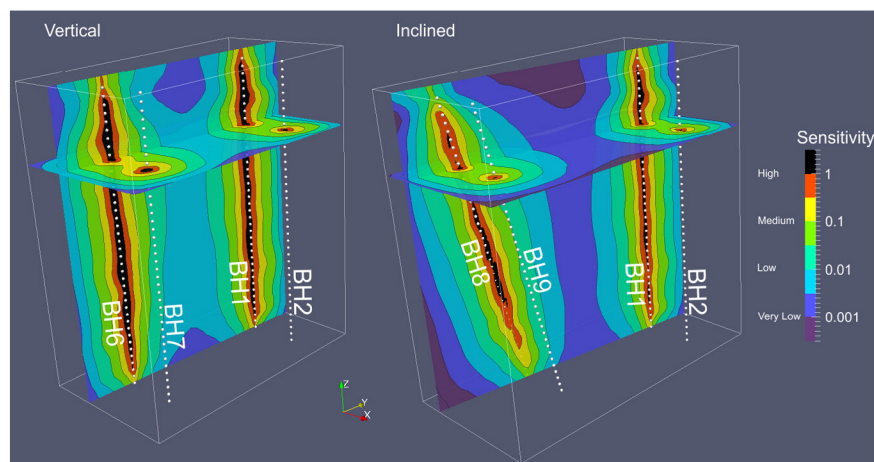


Fig. 3. Cumulative sensitivity patterns for the vertical (left) and inclined ERT cross-borehole imaging cells (right).

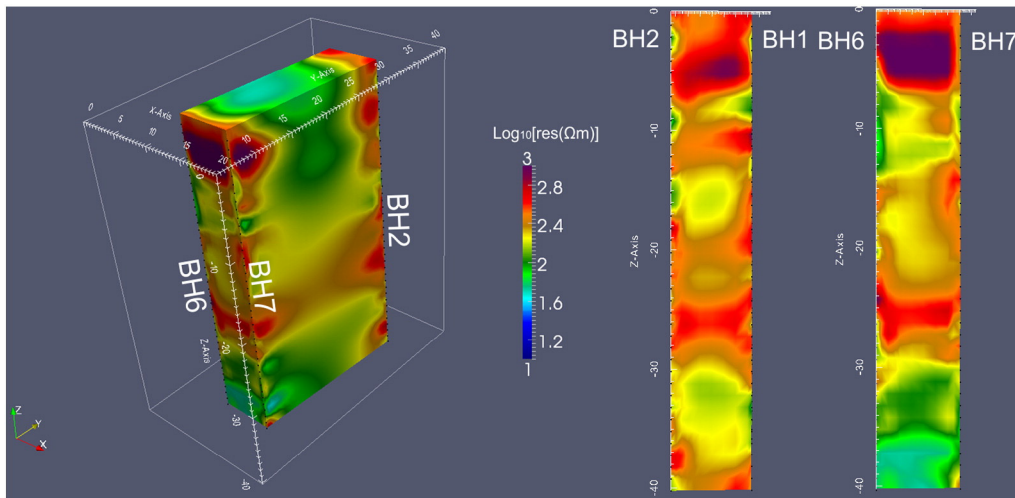


Fig. 4. Baseline 3D resistivity image of the ERT Trial area (left), and 2D crosshole panels (right) on the building side (BH1–2) and away from the building (BH6–7).

simulant. No appreciable decay of the conductive plume signature was observed over the space of ~ 10 weeks of routine monitoring following the end of the Stage 1 injection, which indicates either long residence times of the plume itself or the retention of residual conductivity in the vadose zone pore spaces after the main plume had passed. The conductive changes towards the base of the images are unconnected; they are thought to be due to seasonal variations in the electrical conductivity of the regional groundwater body (lower Quaternary plus sandstone bedrock aquifer), which is separated from the upper aquifer by a low permeability till layer (Fig. 1).

We found that ERT inversion was essential for this interpretation, as the statistics of conductive changes in the raw resistance data relative to the baseline alone could not be attributed unambiguously to the injection. Instead, we observed much stronger correlation of such changes with unrelated (but clearly relevant) processes in the near surface such as rainfall and subsequent infiltration into the vadose zone (see quiescent baseline), surface runoff, and infiltration of dissolved road

de-icing salt following snowfall, and variations in ground temperature driven by air temperature changes and natural gradients in the subsurface. Furthermore, statistical analysis alone is unable to provide spatial information; leak path geometry can only be recovered through inverse modelling of the subsurface.

3.2.3. Stage 2 injection

For this stage, simulant with the lowest conductivity contrast was injected into BH4 at the same low leak rate used in Stage 1, partly to assess the extent to which ERT could distinguish separate events in a 'leak-on-leak' scenario. However, expectations were modest as the Stage 2 plume behavior was likely to be complex, and leak-on-leak scenarios had not been simulated prior to the experiment. Once again, no significant response was noted for a period of at least ~ 4 weeks. Further negative changes (i.e. relative increases in conductivity) were imaged eventually (Fig. 5c), which, compared with Stage 1, had increased in strength and appeared in new regions, consistently enveloping the

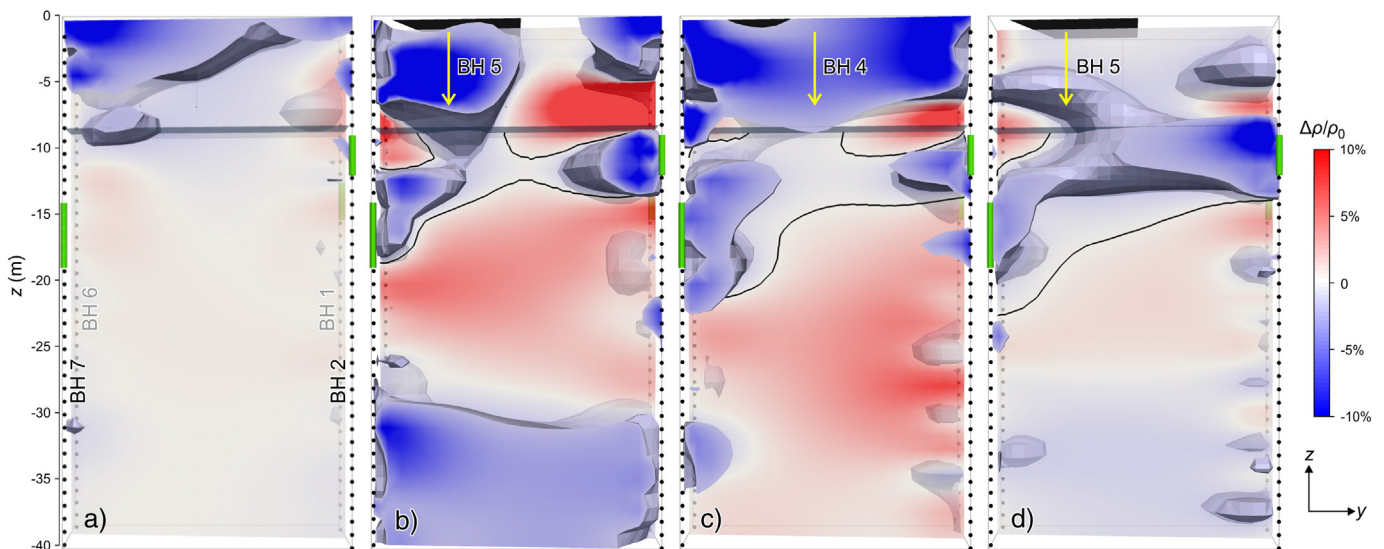


Fig. 5. 3D fractional resistivity change (resistivity change $\Delta\rho$ divided by baseline resistivity ρ_0) images showing changes observed during the quiescent baseline period (a), and as a result of the Stage 1 (b), Stage 2 (c) and Stage 3 (d) injections. Results are obtained by performing 4D inverse modelling at regular intervals, and plots show % changes relative to the inverted model at the start of the most recent injection stage (change $\Delta\rho$ in inverted resistivity at time t divided by inverted resistivity ρ_0 at baseline time). Baseline dates are 13th Jan. 2013 for quiescent baseline, 5th Feb. 2013 for Stage 1, 28th May 2013 for Stage 2, 16th Sep. 2013 for Stage 3. Approximate locations of injections are shown by yellow arrows. Red indicates resistive changes, i.e. increases relative to baseline resistivity, while blue reflects conductive changes. The black line is the 0% change contour, which is assumed to delineate the inferred pathway; green cylinders show windows of historic contamination found in sediment cores from ERT boreholes. (For interpretation of the references to color in this figure legend, the reader is referred to the web version of this article.)

Stage 1 plume volume. This evidence demonstrates the successful detection of the lower contrast Stage 2 leak against the background of the Stage 1 leak, which was a welcome result, given the challenges of detecting a low-contrast tracer in a pathway already occupied by the stronger previous tracer.

3.2.4. Stage 3 injection

This final stage involved the introduction of simulant with a significantly higher conductivity and at a high leak rate, reflecting the most pessimistic leak scenario. Stage 3 was designed to corroborate the results of the previous two stages, as it was expected that the existing flow path would be reoccupied once more and that the cumulative effect of the more conductive simulant would overcome the limitations of the low-sensitivity array geometry, by consistently highlighting flow paths throughout the ERT model. The Stage 3 injection lasted three days, during which approximately 34 m³ of simulant were released into the vadose zone via BH5. Resistivity ratio images for Stage 3 responded very quickly (~1 week) after the injection event, and the change evolution over the subsequent 6 weeks showed that the Stage 1 flow path was indeed occupied once again (Fig. 5d). The resistivity ratio isosurface indicating a 2% conductive change was now connected

across the model and provided an intuitive visual representation (as well as a quantitative measure) of inferred fluid flow in the shallow subsurface beneath the experimental area. More detailed quantitative interpretation is difficult without knowledge of hydraulic properties of the pathway and the subsurface adjacent to (but outside) the imaging volume. The cumulative nature of the injections and uncertain residence times in the unsaturated zone add complexity. It is also likely that the higher injection rate of the Stage 3 injection will create stronger hydraulic gradients, forcing the simulant to dissipate more rapidly into the preferential pathway compared to Stages 1 and 2. This may also cause a larger proportion of the simulant to exit the volume imaged by the borehole sensor array and thus become invisible to the present experimental setup. A more comprehensive monitoring deployment comprising multiple adjacent imaging cells would address this shortfall.

3.3. Extended baseline monitoring and full trial analysis

After the staged injections, ERT monitoring continued for a further 12 months with the aim of tracking the fate of the simulant plume, that was expected to decay and disperse over time. Our goal was to explore current practical limits of our inversion strategy that required

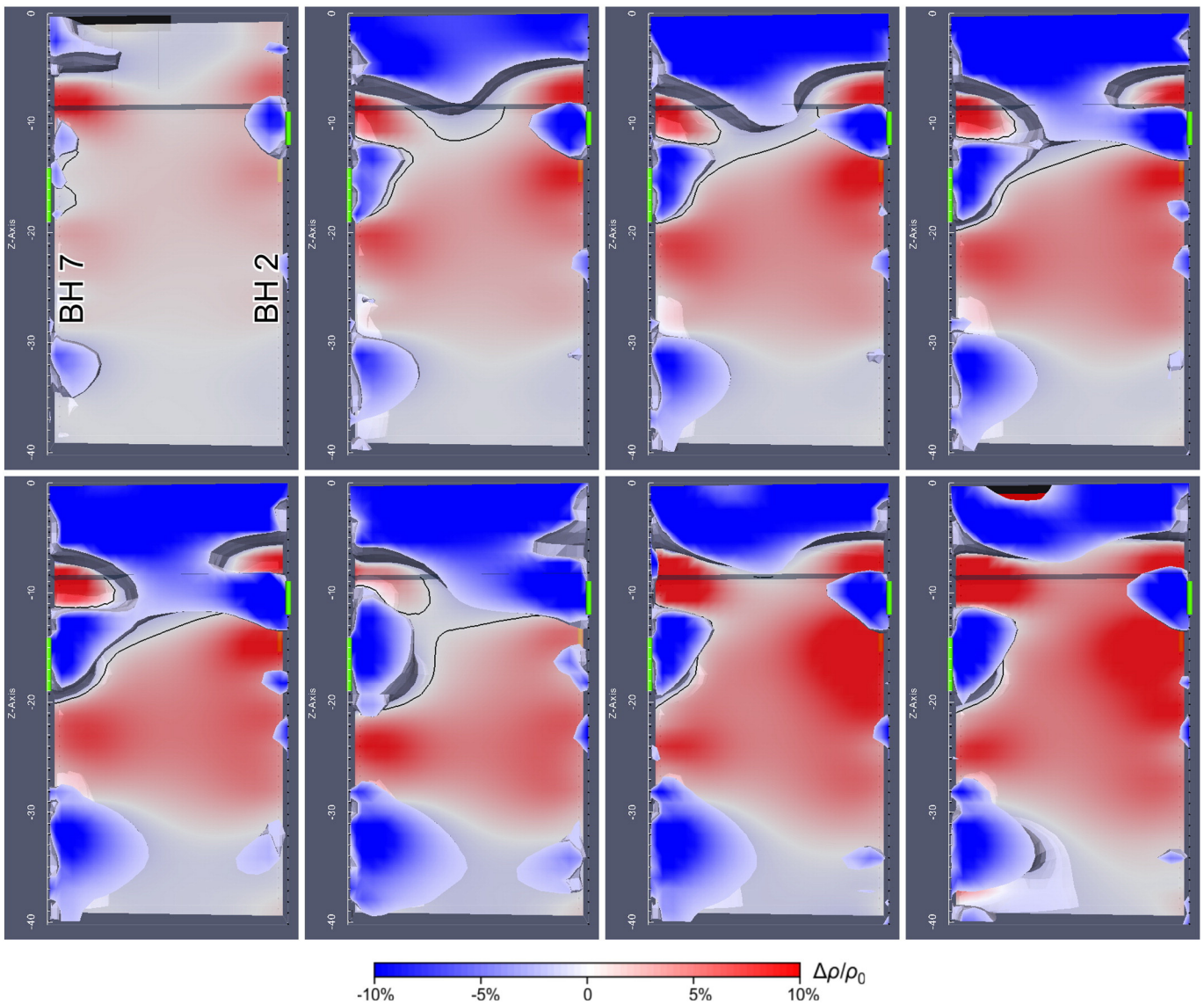


Fig. 6. Entire monitoring sequence fractional resistivity changes in inverted vertical cell images for 28th Mar. 2013, 28th May 2013, 18th Jul. 2013, 13th Sep. 2013, 4th Nov. 2013, 10th Mar. 2014, 27th Jul. 2014, 2nd Dec. 2014 (left-to-right, top-to-bottom). Changes plotted relative to 5th Feb. 2013, no BH1 data used. Contours at the approximate boundaries of conductive changes highlight the inferred preferential pathway over time.

simultaneous 4D inversion of a time series of consecutive 3D datasets. It was found that, given the density and nature of the ERT monitoring data, a sequence of not more than 48 full datasets, spread approximately evenly throughout the full duration of the trial, could be simultaneously inverted with the available algorithm and computational resources. Typical inversion times for full 48-dataset inversions were below 22 h. Given that data acquisition itself requires ~24 h per imaging cell and data pre-processing time was negligible, a typical time frame of <48 h from start of data acquisition to an inverted result was achievable. This was deemed sufficient to provide adequate temporal resolution for leak events within the suspected range of leak rates, and at the same time allow detection of subtle changes in subsurface properties and structure over relevant time periods of many months. For a larger monitoring system comprising multiple imaging cells the overall numerical demands would increase significantly, but inversion strategies could be tailored to cover partial imaging volumes at a time, whilst computational resources could be increased.

An issue with noticeable distortion of the original Stage 2 image (not shown) in the vicinity of BH1, was found to be due to water ingress in an electrical connector on BH1 at the surface that had suffered mechanical damage from activity unrelated to the ERT experiment. It was not possible to repair the connector for the remainder of the experiment. Therefore to investigate the full duration of the experiment, including the three injection stages and the monitoring of the fate of the tracers, all data involving any BH1 electrode was removed from the inversion. A subset of the resulting change images for the entire monitoring period of ~2 years is shown in Fig. 6.

3.4. Revised geological model and enhanced conceptualization

A revised geological model of the MSSS area was built using existing stratigraphic information from around 190 boreholes in

the wider Sellafield Separation Area, combined with new lithology data from the eight ERT trial boreholes. The model was generated using the GSI3D software and workflow (Kessler et al., 2009) and comprises around 30 geological cross-sections, which were defined using boreholes from the above dataset and manually correlated using a modelling lithostratigraphy based on the 16 separate geological units described earlier (Table S1, Supplementary information). The resulting model is a fully digital 3D spatial model of the lithostratigraphy in the study area; it can thus be interrogated at arbitrary locations to create synthetic borehole logs. We found that this form of structural correlation across the trial area offered enhanced spatial context and new conceptual understanding of the relationships between sand-dominated and gravel-dominated facies and the clay-rich till layers present in the area. Crucially, it also allowed direct and interactive comparison between the interpreted geology, measured electrical properties and hydrogeological monitoring information. Fig. 7 presents the % change ERT image following the Stage 1 injection, superimposed on a geological cross-section through the trial area, which shows the lithostratigraphic context in the region between boreholes BH7 and BH1. Amongst other features, the section shows the laterally coherent 'Glacial till extensive aquitard unit' ('Lower Till 1', light blue) extending across the entire section at approximately constant depth (~23 m bgl). It is thought that this low-permeability layer is responsible for providing a high degree of hydraulic separation between the upper and lower groundwater systems, as observed in previous studies (El-Ghonemey, 2004). Other till units are clearly not as extensive and appear to provide more localized hydraulic barriers, potentially diverting or retarding flow in a particular direction. One example is the 'Glacial till local aquitard unit' observed at ~12 m bgl in BH7 ('Upper Till 2'), which appears to locally divert flow in the inferred pathway downwards (Fig. 7).

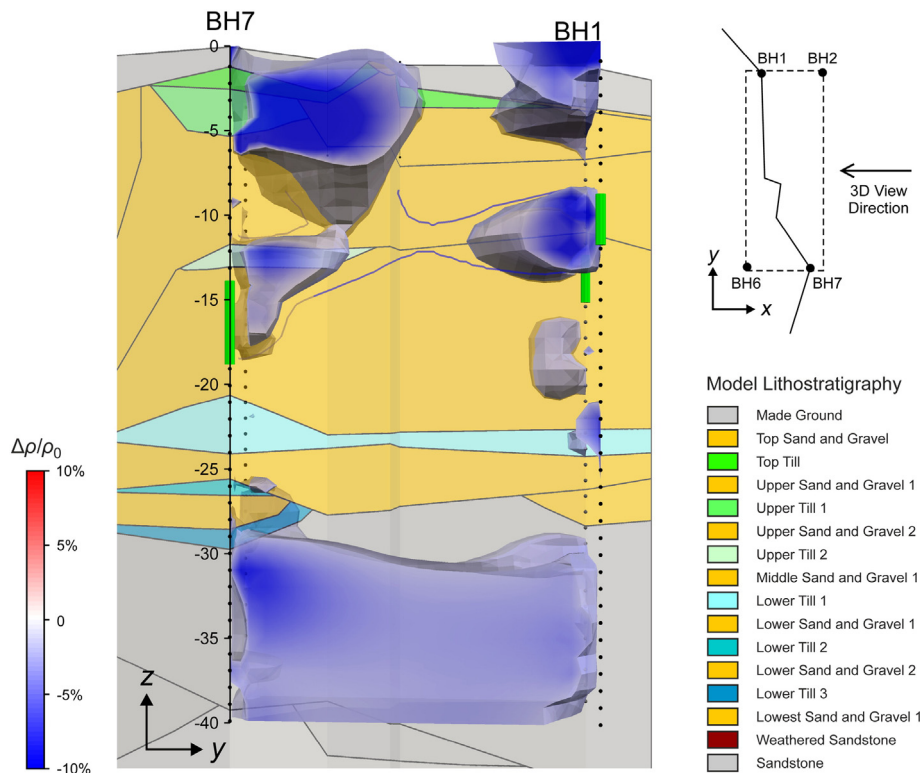


Fig. 7. Spatial correlation of geoelectrical monitoring results with the revised 3D geological model of the experimental area. Fractional resistivity change image following Stage 1 injection superimposed on geological cross-section through BH9–BH710205–BH1. Green cylinders along the boreholes indicate regions of historic contamination detected in sediment cores. The solid blue contour line in the resistivity image reflects the 0% change boundary and serves to outline the inferred preferential pathway. (For interpretation of the references to color in this figure legend, the reader is referred to the web version of this article.)

4. Conclusions

Automated ERT monitoring was applied at a UK nuclear licensed site for the first time and a full-scale field experiment trialing the methodology at MSSS in Sellafield successfully detected, characterized, and tracked simulated leaks. Contrary to experience obtained by previous studies under more favorable conditions at US sites, at Sellafield we were unable to discriminate simulated leaks from unrelated processes using simple metrics based on raw data statistics alone. Instead, we have shown in this study that careful experimental design and full 4D ERT imaging can overcome the lack of sensitivity associated with challenging borehole sensor geometries and the poor property contrasts presented by UK Quaternary geology. Images of resistivity changes relative to a baseline date prior to a leak have revealed likely pathways of simulant flow in the vadose zone and upper groundwater system. The geophysical evidence was found to be compatible with historic contamination detected in permeable facies in borehole sediment cores, and with a geological model based on wider scale borehole stratigraphy. Results showed that laterally discontinuous till units forming localized hydraulic barriers can substantially affect flow patterns and contaminant transport in the shallow subsurface at Sellafield. Thus, when compared with traditional methods of leak detection at nuclear sites, only geophysical imaging (of the kind presented here, but not necessarily limited to ERT) can provide the detailed spatial and temporal information at the (sub-meter) scale needed to reduce uncertainty in models of subsurface processes, particularly where they underpin decision-making in nuclear risk management. Our experiment at one of the most challenging nuclear legacy facilities in the world has shown how routine operation of a permanent ERT monitoring system could support critical decommissioning activities over the coming decades. Full-scale permanent systems covering entire buildings or subsurface structures would require about an order-of-magnitude more boreholes and ERT sensors, and a proportionally higher effort in terms of data collection and processing, thus setting new challenges for the future direction of R&D in geoelectrical monitoring.

Acknowledgments

This paper is published with the permission of the Executive Director of the British Geological Survey (NERC) and Sellafield Ltd. (on behalf of the Nuclear Decommissioning Authority). Arnaud Watlet and Peter Bergmann provided detailed reviews that helped improve an earlier version of the manuscript.

Appendix A. Supplementary information

Supplementary information to this article can be found online at <http://dx.doi.org/10.1016/j.scitotenv.2016.04.212>.

References

BNFL, 1998. Engineering developing Sellafield drypack process with world in mind. Nuclear Engineering International, Global Trade Media, London Available from <http://www.neimagazine.com/features/featurebnfl-engineering-developing-sellafield-drypack-process-with-world-in-mind/> (accessed 29 March 2016).

BNFL, 2006. Decommissioning B38. New Civil Engineer, Emap, London, Available from <http://www.newcivilengineer.com/decommissioning-b38/484772.article> (accessed 29 March 2016).

Baldwin, N.D., 2003. Remediating Sellafield - A New Focus for the Site. Waste Management (WM) Conference. WM Symposia, Tucson, AZ.

Barnett, D.B., Gee, G.W., Sweeney, M.D., Johnson, M.D., Medina, V.F., Mendoza, D.P., et al., 2003. Results of Performance Evaluation Testing of Electrical Leak-Detection Methods at the Hanford Site Mock Tank - FY 2002-2003 Pacific Northwest National Laboratory.

Binley, A., Hubbard, S.S., Huisman, J.A., Revil, A., Robinson, D.A., Singha, K., et al., 2015. The emergence of hydrogeophysics for improved understanding of subsurface processes over multiple scales. *Water Resour. Res.* 51, 3837-3866.

Calendine, S., Rucker, D.F., Fink, J.B., Levitt, M.T., 2011. Automated leak detection of buried tanks using geophysical methods at the Hanford Nuclear site. Symposium on the Application of Geophysics to Engineering and Environmental Problems. EEGS, Charleston, SC.

Chambers, J.E., Wilkinson, P.B., Weller, A.L., Meldrum, P.I., Gilvy, R.D., Caunt, S., 2007. Mineshaft imaging using surface and crosshole 3D electrical resistivity tomography: a case history from the East Pennine Coalfield, UK. *J. Appl. Geophys.* 62, 324-337.

Cruikshank, J., 2012. Findings of the Sellafield Contaminated Land & Groundwater Management Project and the Next Steps for the Land Quality Programme. Land Quality Report, Sellafield Ltd.

Cummings RLK, 2012. Options for Leak Management from Nuclear Legacy Facilities during Decommissioning. Royal Holloway University of London. p. 91.

Daily, W., Ramirez, A., Binley, A., 2004. Remote monitoring of leaks in storage tanks using electrical resistance tomography: application at the Hanford Site. *J. Environ. Eng. Geophys.* 9, 11-24.

Dewey, G., Atherton, N., Ball, T., Kuras, O., Wilkinson, P., Meldrum, P., 2014. The Ground Environment Management Scheme (GEMS): Development of Technologies for Detecting and Monitoring Subsurface Leakage and Contaminant Transport, Supporting the Decommissioning of Legacy Silos at the Sellafield Site, UK. Waste Management (WM) Conference. WM Symposia, Phoenix, AZ. p. 14160.

El-Ghonemey, H., 2004. SCLS Groundwater Conceptual Model. Nuclear Sciences and Technology Services. BNFL.

Emptage, M., Hepworth, S., Winspear-Roberts, V., Cummings, R., 2013. The leak management hierarchy. Decommissioning Challenges: An Industrial Reality and Prospects. Société Française d'Énergie Nucléaire, Avignon, France.

Johnson, T.C., Slater, L.D., Ntarlagiannis, D., Day-Lewis, F.D., Elwaseif, M., 2012a. Monitoring groundwater-surface water interaction using time-series and time-frequency analysis of transient three-dimensional electrical resistivity changes. *Water Resour. Res.* 48.

Johnson, T.C., Versteeg, R.J., Rockhold, M., Slater, L.D., Ntarlagiannis, D., Greenwood, W.J., et al., 2012b. Characterization of a contaminated wellfield using 3D electrical resistivity tomography implemented with geostatistical, discontinuous boundary, and known conductivity constraints. *Geophysics* 77, En85-En96.

Kessler, H., Mathers, S., Sobisch, H.G., 2009. The capture and dissemination of integrated 3D geospatial knowledge at the British Geological Survey using GSI3D software and methodology. *Comput. Geosci.* 35, 1311-1321.

Kim, J.H., Yi, M.J., Park, S.G., Kim, J.G., 2009. 4-D inversion of DC resistivity monitoring data acquired over a dynamically changing earth model. *J. Appl. Geophys.* 68, 522-532.

Kuras, O., Pritchard, J.D., Meldrum, P.I., Chambers, J.E., Wilkinson, P.B., Ogilvy, R.D., et al., 2009. Monitoring hydraulic processes with automated time-lapse electrical resistivity tomography (ALERT). *Comput. Rendus Geosci.* 341, 868-885.

Kuras, O., Wilkinson, P.B., White, J.C., Chambers, J.E., Meldrum, P.I., Ogilvy, R.D., 2011. MSSS Leak Mitigation - Leak Detection Phase 3: Desk Study for ERT Technology. Commissioned Report CR/11/053. British Geological Survey.

LaBrecque, D.J., Miletto, M., Daily, W., Ramirez, A., Owen, E., 1996a. The effects of noise on Occam's inversion of resistivity tomography data. *Geophysics* 61, 538-548.

LaBrecque, D.J., Ramirez, A.L., Daily, W.D., Binley, A.M., Schima, S.A., 1996b. ERT monitoring on environmental remediation processes. *Meas. Sci. Technol.* 7, 375-383.

Loke, M.H., Chambers, J.E., Rucker, D.F., Kuras, O., Wilkinson, P.B., 2013a. Recent developments in the direct-current geoelectrical imaging method. *J. Appl. Geophys.* 95, 135-156.

Loke, M.H., Dahlin, T., Rucker, D.F., 2013b. Smoothness-constrained time-lapse inversion of data from 3D resistivity surveys. *Near Surf. Geophys.* <http://dx.doi.org/10.3997/1873-0604.2013025>.

Mankins, J.C., 1995. Technology Readiness Levels - A White Paper. Office of Space Access and Technology, NASA.

McGillivray, P.R., Oldenburg, D.W., 1990. Methods for calculating Fréchet derivatives and sensitivities for the nonlinear inverse problem - a comparative-study. *Geophys. Prospect.* 38, 499-524.

Merritt, J.W., Auton, C.A., 2000. An outline of the lithostratigraphy and depositional history of Quaternary deposits in the Sellafield district, west Cumbria. *Proc. Yorks. Geol. Soc.* 53, 129-154.

Nuclear Decommissioning Authority, 2011. NDA Strategy, Effective from April 2011. United Kingdom Nuclear Decommissioning Authority.

Ogilvy, R.D., Meldrum, P.I., Kuras, O., Wilkinson, P.B., Chambers, J.E., Sen, M., et al., 2009. Automated monitoring of coastal aquifers with electrical resistivity tomography. *Near Surf. Geophys.* 7, 367-375.

Okay, G., Leroy, P., Ghorbani, A., Cosenza, P., Camerlynck, C., Cabrera, J., et al., 2014. Spectral induced polarization of clay-sand mixtures: experiments and modeling. *Geophysics* 79, E353-E375.

Ramirez, A., Daily, W., Binley, A., LaBrecque, D., Roelant, D., 1996. Detection of leaks in underground storage tanks using electrical resistance methods. *J. Environ. Eng. Geophys.* 1, 189-203.

Rucker, D.F., Levitt, M.T., Myers, D.A., Henderson, C., 2008. Development of an Electrical Resistivity Imaging Program for Subsurface Characterization at Hanford. Waste Management (WM) Conference. WM Symposia, Phoenix, AZ. p. 8193.

Slater, L.D., Ntarlagiannis, D., Day-Lewis, F.D., Mwakanyamale, K., Versteeg, R.J., Ward, A., et al., 2010. Use of electrical imaging and distributed temperature sensing methods to characterize surface water-groundwater exchange regulating uranium transport at the Hanford 300 Area, Washington. *Water Resour. Res.* 46.

Smith, N., Cooper, S., 2004. SCLS Phase 1 - Sellafield Geological Conceptual Model. Nuclear Sciences and Technology Services. British Nuclear Fuels Limited (BNFL).

Truex, M.J., Johnson, T.C., Strickland, C.E., Peterson, J.E., Hubbard, S.S., 2013. Monitoring vadose zone desiccation with geophysical methods. *Vadose Zone J.* 12.

Wilkinson, P.B., Meldrum, P.I., Kuras, O., Chambers, J.E., Holyoake, S.J., Ogilvy, R.D., 2010. High-resolution electrical resistivity tomography monitoring of a tracer test in a confined aquifer. *J. Appl. Geophys.* 70, 268-276.